



Airlift-driven external-loop tubular photobioreactors for outdoor production of microalgae: assessment of design and performance

F. G. Acien Fernández*, J. M. Fernández Sevilla, J. A. Sánchez Pérez,
E. Molina Grima, Y. Chisti

Department of Chemical Engineering, University of Almería, E-04071 Almería, Spain

Received 5 November 1999; received in revised form 27 September 2000; accepted 7 November 2000

Abstract

A methodology is presented for designing photobioreactors with tubular loop solar receivers in which the fluid is circulated by an airlift device. The design method effectively combines the relevant aspects of external irradiance-dependent cell growth, oxygen accumulation in the solar loop, oxygen removal in the airlift device, and hydrodynamics of the airlift system that determine the flow velocity through the solar receiver. The design approach developed was used to model and build a 0.2 m³ outdoor photobioreactor. A compact degasser in the airlift section eliminated dead zones and dark zones, while achieving complete separation of gas and liquid. The measured gas–liquid hydrodynamics, mass transfer, and culture productivity were consistent with the model predictions. The reactor was tested with continuous culture of the microalga *Phaeodactylum tricornerutum* at various liquid velocities through the tubular solar receiver. A biomass productivity of 1.20 g l⁻¹ d⁻¹ (or 20 g m⁻² d⁻¹) was obtained at a dilution rate of 0.050 h⁻¹. Solar receiver linear liquid velocities of 0.50 and 0.35 m s⁻¹ gave similar biomass productivities, but the culture collapsed at lower velocities. An adverse effect of high dissolved oxygen concentration on productivity was observed. Oxygen accumulation could be reduced by increasing the liquid velocity and this enhanced the biomass yield. © 2001 Elsevier Science Ltd. All rights reserved.

1. Introduction

Microalgae have been cultured by mankind for centuries, mainly as food; however, systematic mass culture methods for potential use in producing high-value algal chemicals were developed more recently (Burlew, 1953). Most of the developmental effort has focused on technologies for open outdoor mass culture. Large-scale production facilities based on open culture methods are in operation in the United States, Australia, and elsewhere. Such systems are economic, but they do not assure a contamination-free monoalgal operation. Fully closed tubular photobioreactors are potentially attractive for large-scale culture that is free of contaminants (Gudin & Chaumont, 1983; Torzillo, Pushparaj, Bocci, Balloni, Materassi, & Florenzano, 1986). Closed devices are undoubtedly more expensive to build and maintain, but they may be the only option for producing certain

potential therapeutics. A variety of closed photobioreactors have been tested or proposed for generating microalgal biomass (Molina Grima, 1999; Tredici, 1999). However, only a few engineering analyses of such reactors have been published (Aiba, 1982; Pirt et al., 1983; Erickson & Lee, 1986; Weissman, Goebel, & Benemann, 1988; Acien Fernández, García Camacho, Sánchez Pérez, Fernández Sevilla, & Molina Grima 1998; Rorrer & Mullikin, 1999). Here we provide a method for designing airlift-driven tubular photobioreactors with continuous run solar loop tubing. Effects of tube length, flow velocity, the airlift column height, and the geometric configuration of the solar receiver on various performance parameters are examined. A photobioreactor designed using the developed approach is proved for culture of the microalga *Phaeodactylum tricornerutum*.

2. The design strategy

An airlift-driven photobioreactors with a continuous run tubular solar receiver essentially consists of two

* Corresponding author. Tel.: + 34-9-50-215484; fax: + 34-9-50-215484.

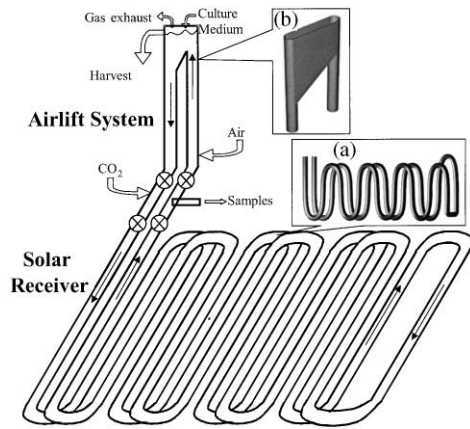


Fig. 1. The outdoor culture system with details of the solar loop (a) and the degasser zone (b).

parts, the airlift system and the looped solar receiver (Fig. 1). The airlift device serves to circulate the culture through the solar receiver. A gas–liquid separator in the upper zone of the airlift column prevents gas bubbles from recirculating into the solar loop. As photosynthesis occurs in the solar tubing, oxygen accumulates and it is stripped out in the airlift zone when the fluid returns from the solar loop. The relevant design aspects are discussed next, separately for the two zones.

2.1. The tubular solar receiver

The variable that must be optimized in design and scale-up of a photobioreactor for continuous production of microalgae is the biomass productivity. The biomass productivity is a function of the growth rate and the biomass concentration; under given conditions, the volumetric productivity P_{bv} is

$$P_{bv} = \mu C_b, \quad (1)$$

where μ is the specific growth rate and C_b is the concentration of the biomass. For a fixed biomass concentration, the growth rate depends on the average irradiance I_{av} inside the reactor. The specific growth rate may be correlated with the average irradiance (Molina Grima et al., 1994a) as follows:

$$\mu = \frac{\mu_{\max} I_{av}^n}{I_k^n + I_{av}^n}. \quad (2)$$

In Eq. (2), μ_{\max} is the maximum specific growth rate, I_k is a constant dependent on algal species and culture conditions, and n is an empirically established exponent. The average irradiance inside a culture may be estimated (Alfano, Romero, & Cassano, 1986; Ación Fernández, García Camacho, Sánchez Pérez, Fernández Sevilla,

& Molina Grima, 1997) using the equation

$$I_{av} = \frac{I_0}{\phi_{eq} K_a C_b} [1 - \exp(-\phi_{eq} K_a C_b)], \quad (3)$$

where K_a is the extinction coefficient of the biomass, I_0 is the irradiance on the culture surface, and ϕ_{eq} is the length of the light path from the surface to any point in the bioreactor. For outdoor placed tubular systems, ϕ_{eq} is related with the tube diameter ϕ and the angle of declination (θ) of the Sun from the vertical (Ación Fernández et al., 1997); thus

$$\phi_{eq} = \frac{\phi}{\cos \theta}. \quad (4)$$

Thus, from a knowledge of the characteristics parameters of the algal strain (i.e., μ_{\max} , K_a , I_k , and n) and using Eqs. (1)–(4), the biomass productivity may be established for any combination of external irradiance and the diameter of solar receiver tubes. Once the volumetric productivity has been determined, the areal productivity P_{ba} is easily calculated as follows:

$$P_{ba} = P_{bv} \frac{\pi \phi^2}{4n_T \phi} = P_{bv} \frac{\pi \phi}{4n_T}, \quad (5)$$

where the separation between the adjacent parallel rungs of the continuous run looped tubing is expressed as a function of the tube diameter (i.e., separation = $n_T \cdot \phi$), with n_T being the number of diameters of separation.

For maximizing the biomass productivity, the irradiance on the surface of the solar tubes must be maximized. This external surface irradiance depends mainly on the solar irradiance, which is a function of the location and the weather conditions (Incropera & Thomas, 1978). For a given location and weather, the geometric arrangement of the solar receiver tubes also determines the irradiance on the surface of the tubes and so does the albedo effect (irradiance enhancement because of reflectance) of the surrounding. The geometric distribution of the tube over a given land surface controls the extent of mutual shading. To maximize land use, a two level loop design (Fig. 1a) with one layer of tubes placed below a first layer is preferred, as used by Torzillo, Carozzi, Pushparaj, Montaini, and Materassi (1993). In this configuration, the lower loop is displaced horizontally with respect to the upper one, so that all tubes are visible when viewed from directly overhead.

Liquid flow velocity in the solar tubular loop must be sufficiently high to ensure a turbulent flow so that cells do not stagnate in the darker interior of the tube for long. However, excessive turbulence can damage cells and this poses an upper limit on the culture velocity. In general, the energy input in the tube and the airlift zone should be such that the dimensions of the microeddies do not approach cellular dimensions. The length scale of the microeddies may be estimated by applying

Kolmogoroff's theory of local isotropic turbulence (Kawase & Moo-Young, 1990); thus

$$\lambda = \left(\frac{\mu_L}{\rho} \right)^{3/4} \xi^{-1/4}, \quad (6)$$

where λ is the microeddy length, ξ is the energy dissipation per unit mass, μ_L is the viscosity of the fluid, and ρ is the fluid's density. The specific energy dissipation rate within the tube depends on the pressure drop, or

$$\xi = \frac{2C_f U_L^3}{\phi}, \quad (7)$$

where C_f is the Fanning friction factor and U_L is the superficial velocity of the liquid in the tube. The friction factor may be estimated using the Blasius equation:

$$C_f = 0.0791 Re^{-0.25}, \quad (8)$$

where Re is the Reynolds number calculated as follows:

$$Re = \frac{\rho U_L \phi}{\mu_L}. \quad (9)$$

Thus, for any selected value of the liquid velocity that can be generated by the airlift device, a value of λ can be calculated. The design must ensure that λ remains greater than the dimensions of the algal cells, whereas the Reynolds number should exceed about 3000 so that the flow is turbulent.

As noted earlier, the maximum continuous run length of the solar tube is limited by a combination of the acceptable upper limit on the dissolved oxygen concentration, the liquid velocity through the tube, and the rate of photosynthesis (Mazzuca Sobczuk, García Camacho, Camocho Rubio, Acien Fernández, & Molina Grima, 2000). The tube length L may be shown to be:

$$L = \frac{U_L ([O_2]_{in} - [O_2]_{out})}{R_{O_2}}, \quad (10)$$

where U_L is the maximum permissible culture velocity established by the cell damage considerations. In Eq. (10), the oxygen concentration at the entrance of the solar tube is generally the same as the saturation value when the fluid is in equilibrium with the atmosphere, and $[O_2]_{out}$ is the maximum acceptable dissolved oxygen concentration that does not inhibit photosynthesis. R_{O_2} is the volumetric rate of oxygen generation by photosynthesis in the tube.

2.2. The airlift system

In addition to satisfying the principal demands of effectively circulating the fluid and achieving the requisite removal of oxygen, the airlift device must have a small volume compared to that of the solar loop so that the

fluid spends less time in this relatively darker region of the bioreactor. These demands are met by having the riser and downcomer tubes of the airlift device as vertical extensions of the ends of the solar loop. The volume in the gas-liquid separator is minimized if the spacing between the parallel walls of the separator (Fig. 1b) is the same as the diameter of the riser or the downcomer. This arrangement also improves light penetration in the degassing zone. Permanent settling of solids is prevented by slanting the floor of the separator at $> 60^\circ$ relative to the horizontal.

To achieve effective separation of gas and liquid, the distance between the entrance and the exit of the degasser should be such that the smallest bubbles have a sufficient time to disengage before the fluid enters the downcomer (Chisti & Moo-Young, 1993). Thus, the time taken by the fluid to traverse the length of the degasser must be greater than or equal to time required by the bubbles to rise out of the fluid. Because all fluid entering the degasser through the riser tube moves through the cross section of the degasser, we have

$$U_L A_r = U_{LD} A_D, \quad (11)$$

where A_r is the cross-sectional area of the riser tube, A_D is the cross-sectional area of the degassing zone, and U_{LD} is the superficial liquid velocity in the degasser. When the parallel degasser walls are spaced a distance ϕ apart, the area A_D equals $h_D \cdot \phi$, where h_D is the height of fluid in the degasser zone. To satisfy the disengagement criterion (Chisti & Moo-Young, 1993), the length L_D of the degasser is governed by the relationship:

$$\frac{L_D}{U_{LD}} \geq \frac{h_D}{U_b}, \quad (12)$$

where U_b is the bubble rise velocity. Because $h_D = A_D/\phi$, substitution of Eq. (11) in Eq. (12) provides the equation

$$L_D = \frac{U_L A_r}{\phi U_b} = \frac{\pi \phi U_L}{4 U_b}. \quad (13)$$

A bubble rise velocity of 0.1 m s^{-1} was used in Eq. (13) to obtain the minimum length L_D .

The liquid flow in the solar receiver is driven by the airlift pump. For a water-like fluid such as the microalgal broth, the induced flow velocity depends mainly on the geometric configuration of the circulation loop and the difference in gas holdup in the riser and the downcomer zones of the airlift column. This relationship has been established (Chisti, 1989) to be:

$$U_L = \sqrt{\frac{2g(\varepsilon_r - \varepsilon_d)h_r}{K_T/(1 - \varepsilon_r)^2 + K_B(A_r/A_d)^2/(1 - \varepsilon_d)^2}}, \quad (14)$$

where K_T and K_B are the frictional loss coefficients for the top and the bottom connecting sections, respectively,

of the airlift loop. Eq. (14) is based on principles of energy conservation and it has been repeatedly validated for a broad range of scales and configurations of airlift devices (Chisti, 1989). In Eq. (14) h_r is the height of the riser section, A_r and A_d are the cross-sectional areas of the riser and the downcomer, ε_r is the gas holdup in the riser, and ε_d is the holdup in the downcomer. Generally, K_T is much smaller than K_B , hence K_T can be neglected (Chisti, 1989). This is particularly true of the loop configuration used for photobioreactors. Because the bottom section of the loop is simply a continuous pipe (the solar receiver), the frictional loss coefficient K_B can be approximated as

$$K_B = 4C_f \frac{L_{\text{eq}}}{\phi}, \quad (15)$$

where C_f is the fanning friction factor established with Blasius equation (Eq. (8)), and L_{eq} is the equivalent length of the loop. The latter is the straight tube length L plus additional length that provides the same pressure drop as all the bends and valves in the loop combined. Because no gas bubbles recirculate, $\varepsilon_d = 0$; hence Eq. (14) with the K_T term neglected and K_B replaced with Eq. (15) becomes

$$U_L = \sqrt{\frac{g\varepsilon_r h_r}{2C_f(L_{\text{eq}}/\phi)}}. \quad (16)$$

Thus, U_L can be estimated if the riser gas holdup (ε_r) is known.

The gas holdup in the riser ε_r , is function of the air flow rate supplied to the riser and also of the liquid flow rate. The relationship between these parameters is the well-known Zuber and Findlay (1965) equation

$$\varepsilon_r = \frac{\beta}{C_0 + (U_b/J_r)} \quad (17)$$

where J_r is the sum of the superficial velocities of the gas and the liquid, β is the ratio of the superficial gas velocity to the total superficial velocity, C_0 is a characteristic parameter, and U_b is the bubble rise velocity. The parameter C_0 is a function of the radial velocity profile; C_0 typically varies from 1.0 to 1.3 as the flow changes from turbulent to laminar. The bubble rise velocity U_b is a function bubble size. For the type of bubbles existing in the riser, the velocity tends to be between 0.2 and 0.4 m s^{-1} . Eqs. (16) and (17) are solved simultaneously to determine the holdup ε_r and the velocity U_L for any specified height h_r of the airlift column. The specific energy input in the reactor may be calculated for any specified volume flow rate Q_G of the injected gas; thus

$$\xi = \frac{P_G}{M} = \frac{Q_G h_r g}{V}, \quad (18)$$

where P_G is the power input due to aeration, M is the mass of culture, and V is the culture volume.

For estimating the gas–liquid oxygen transfer capability of the airlift column, the overall gas–liquid volumetric mass transfer coefficient $k_L a_L$ may be estimated directly using various available correlations (Chisti, 1989, 1999a); however, the reliability of such estimates is often quite poor especially for unusual reactor geometries as was the case here. A more reliable prediction method based on fundamental principles and small-scale experimentation has been demonstrated for several cases (Chisti, 1989, 1999a) and that approach was used here. Thus, the volumetric mass transfer coefficient ($k_L a_L$), the gas holdup (ε_r), the mean bubble diameter (d_B), and the true mass transfer coefficient (k_L) are known to be related (Chisti, 1989) according to the equation:

$$\frac{k_L}{d_B} = \frac{k_L a_L (1 - \varepsilon_r)}{6\varepsilon_r}. \quad (19)$$

Calculations of the k_L/d_B ratio (Eq. 19) from the measured $k_L a_L$ and gas holdup in bubble columns and airlift devices have shown this ratio to be a constant for a given fluid, irrespective of the aeration rate (Chisti & Moo-Young, 1987; Chisti, 1989). For air–water dispersions and for suspensions in which the suspending fluid is water-like, the value of k_L/d_B may be calculated (Chisti, 1989) with the equation

$$\frac{k_L}{d_B} = 5.63 \times 10^{-5} \left(\frac{g D_L \rho^2 \sigma}{\mu_L^3} \right)^{0.5} e^{-0.131 C_s^2}, \quad (20)$$

where C_s is the concentration of solids in suspension (wt/vol%), D_L is the diffusivity of gas in liquid, and σ is the interfacial tension. The k_L/d_B ratio calculated with Eq. (20) could be used in Eq. (19) to determine the $k_L a_L$. The gas holdup ε_r had been determined earlier using Eqs. (16) and (17).

3. Materials and methods

3.1. Organism and culture conditions

Phaeodactylum tricorutum UTEX 640 was the micro-alga used. The cultures were operated as chemostats. Fresh medium was supplied only during the 10-h day-light period and dilution stopped during the night. The photobioreactor was made of Plexiglas. The reactor was located outdoors in Almería (36° 50' N, 2° 27' W), Spain. The cultures were maintained at pH 7.7 by automatically injecting carbon dioxide, as needed. Nutrients limitations were prevented by using the Mann and Myers (1968) medium at three times the normal concentration. The solar receiver loop was submerged in a pond of water held at $20 \pm 2^\circ\text{C}$. The bottom and the inside walls of the pool were painted white to improve reflectance. The liquid velocity in the solar tube varied independently of the dilution rate, from 0.17 to 0.50 m s^{-1} .

The photosynthetic photon flux fluence rate or quantum scalar irradiance I_w , was measured inside the pond using a quantum scalar irradiance meter (QSL-100 Biospherical Instruments Inc., San Diego, CA, USA). This type of sensor measures the photon flux from all directions and it is better suited for systems that operate independently of the geometry of the light field. Because phytoplankton are scalar collectors, and photosynthesis does not depend on the direction from which the photons are received, scalar irradiance is a better measure of the available photon flux (Lassen & Jorgensen, 1994).

3.2. Outdoor photobioreactor

The tubular photobioreactor consisted of a 4 m tall airlift section with a degasser zone as shown in Fig. 1. Air was injected in one of the vertical tubes, or the riser, of the airlift device. Two ends of a continuous run solar receiver tubing were connected to the airlift riser and downcomer sections, respectively. The internal diameter of the tubing of the solar loop, the riser, and the downcomer was the same at 0.053 m. The external tube diameter was 0.06 m. The total reactor volume was 0.2 m³. The continuous run solar loop tubing was arranged in two layers to occupy a compact land area of 12 m². The total run length was 80 m. The adjacent intertube distance in any horizontal plane was 0.09 m. The wall-to-wall vertical distance between the two layers of the loop was 0.03 m. The length of the degasser zone was 0.22 m and its bottom was sloped at an angle of 60° to the horizontal, so that biomass would not settle permanently.

A suitable placement of tubes was established empirically by arranging 0.06 m diameter tubes with blackened surfaces in the configuration of the solar loop and measuring the irradiance on the tube perimeter at 8 equally spaced locations on tubes in both planes (Fig. 2). The measurements were averaged to obtain a mean value, I_{mean} . Irradiance I_w was measured also on the water pool. The mean irradiance on the surface of a tube was normalized with respect to that on the water

pool, to obtain a dimensionless irradiance $I_{\text{normalized}}$. Measurements were made for a total of 18 combinations of vertical distance h and the horizontal tube spacing d (Fig. 2). The d -values tested were 0, 0.03, 0.06, 0.09, 0.12, and 0.15 m; the h -values were 0, 0.03, and 0.06 m.

3.3. The fluid-dynamic parameters

The liquid velocity in the tube was measured by the tracer method. Thus, a pulse of acid/alkali was introduced at the entrance of the tubular loop and detected at the end using a pH electrode. The liquid velocity, U_L , was calculated using the known distance L_t between the tracer injection and detection points (entrance and exit of the solar receiver), and the measured time interval between injection and detection; thus,

$$U_L = \frac{L_t}{t_{mr}}, \quad (21)$$

where t_{mr} was the time interval between injection and detection.

The gas holdup in the riser was measured by the manometric method (Chisti, 1989). Thus, two pressures taps drilled near the top and the bottom of the riser section were connected to an inverted U-tube manometer. From the known vertical distance h_t between the taps, and the manometer reading Δh_m , the holdup was calculated as follows:

$$\varepsilon_r = \frac{\Delta h_m}{h_t}. \quad (22)$$

Because visible gas bubbles did not recirculate, the gas holdup in the downcomer and the loop were negligible, except when the gas was injected in the loop. In the latter case, the gas holdup in the loop was estimated as the ratio of the gas flow rate and the total (gas and liquid) fluid flow in the tube.

The axial dispersion coefficient in individual sections of the reactor was determined using the method of Verlaan, Van Eijs, Tramper, and van't Riet (1989). For this, a pulse of tracer was injected and signals from two probes located downstream at the entrance and exit of each zone (solar loop and the airlift system) were registered on-line. By comparing both signals, the Bodenstein number, Bo , was obtained in each zone and the dispersion coefficient D_z was calculated as follows:

$$D_z = \frac{U_L L_{\text{section}}}{Bo}. \quad (23)$$

3.4. Volumetric mass transfer coefficients

The volumetric gas–liquid mass transfer coefficient was determined in seawater without the cells. The reactor was filled with seawater and liquid circulation was

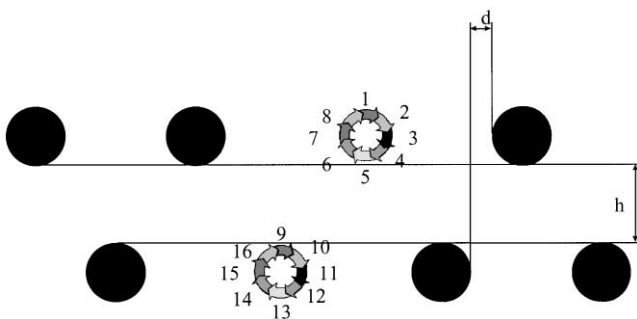


Fig. 2. Solar loop geometry. The vertical distance h and the horizontal spacing d between tubes are shown. Eight measurement points are indicated on the perimeter of tubes for averaging the irradiance received values.

initiated by supplying air in the riser, as in normal culture operations. Once a steady state had been attained, the water became air saturated and the measured concentration of dissolved oxygen was constant at the entrance (i.e., in the degasser zone) and the exit of solar tube. At this point, nitrogen was injected at the inlet of the solar tube. The location of the nitrogen injection point and the flow rate of the gas were identical to those used typically with carbon dioxide during the cultures. Because of stripping of dissolved oxygen by the nitrogen gas, the oxygen concentration at the exit of the solar tube declined continuously until a new steady state had been attained (Camacho Rubio, Ación Fernández, Sánchez Pérez, García Camacho, & Molina Grima, 1999). At this condition, the amount of dissolved oxygen stripped in the solar receiver equaled the amount of oxygen absorbed in the airlift pump (riser and degasser). An oxygen mass balance on the solar receiver could now be established (Camacho Rubio et al., 1999) as follows:

$$Q_L([O_2]_{in} - [O_2]_{out}) = V_L k_L a_L ([O_2^*] - [O_2])_{LM} (1 - \varepsilon_l) \quad (24)$$

In view of the plug flow regime, Eq. (24) employs a logarithmic mean driving force for oxygen transfer, calculated as follows:

$$([O_2^*] - [O_2])_{LM} = \frac{([O_2^*]_{in} - [O_2]_{in}) - ([O_2^*]_{out} - [O_2]_{out})}{\ln([O_2^*]_{in} - [O_2]_{in}) / ([O_2^*]_{out} - [O_2]_{out})} \quad (25)$$

The dissolved oxygen values at the inlet and the outlet of the solar tube were determined experimentally, whereas the equilibrium dissolved oxygen values were established using Henry's law. At the entrance of the solar tube (i.e., the end of the degasser), because pure nitrogen bubbles were present, the dissolved oxygen concentration in equilibrium with the gas phase was zero. At the exit of the solar tube, the mole fraction of oxygen in the nitrogen bubbles needed to be known in order to calculate $[O_2^*]_{out}$. The exit mole fraction of oxygen in the gas phase was calculated using the equation:

$$Q_L([O_2]_{in} - [O_2]_{out}) = F_{N_2} Y_{O_2, out} \quad (26)$$

where F_{N_2} is the molar flow rate of the injected nitrogen and Y_{O_2} is the oxygen-to-nitrogen molar ratio in the gas exiting from the solar receiver tube. Similar balances could be established for the airlift pump and, hence, the $k_L a_{L, airlift}$ in the airlift device (excluding the solar tube) could be determined (Camacho Rubio et al., 1999). Because for the conditions studied the absorption rate was shown to be independent of the chemical reaction taking place in the liquid phase, the $k_L a_{L, CO_2}$ could be directly related to the $k_L a_L$ for oxygen by a single factor ($= 0.93$) that took into account the difference in aqueous diffusivities of the two gases.

4. Results and discussion

4.1. Design of the reactor

Mean annual biomass productivity of *P. tricornutum* at the known optimal dilution rate of 0.040 h^{-1} was simulated using previously established outdoor growth parameters for various conditions of irradiance and solar tube diameters (Ación Fernández et al., 1998). Eqs. (1)–(3) were used for predicting the biomass productivities shown in Fig. 3a. Clearly, as the tube diameter increased, the volumetric productivity of biomass declined for otherwise fixed conditions; however, the areal productivity increased as more culture volume could be accommodated in a given area. Both the volumetric and the areal productivities were similarly sensitive to changes in the tube diameter (Fig. 3a). Too low a volumetric productivity is not wanted as it implies a dilute culture broth and this substantially increases the cost of recovering the biomass, as a greater volume needs to be processed for obtaining a given quantity of cells. In addition, as the tube diameter increased, the energy dissipation per unit mass decreased whereas the range between maximum

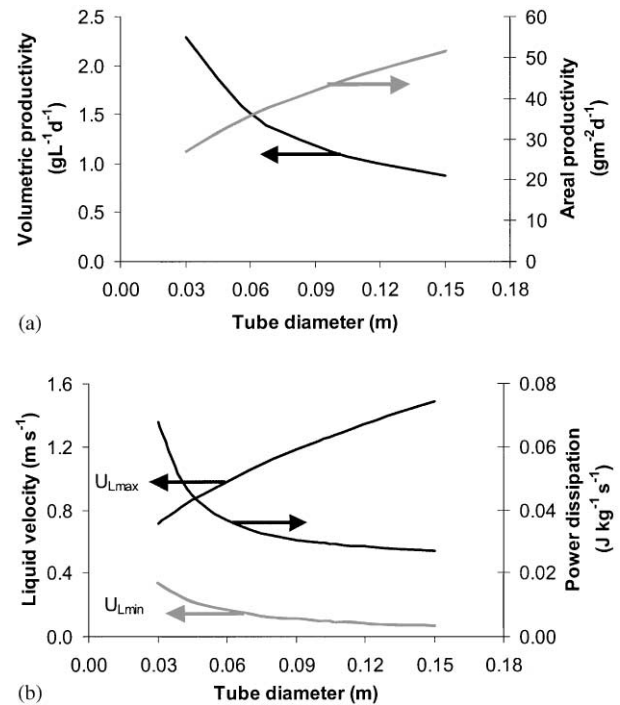


Fig. 3. Influence of tube diameter on: (a) volumetric and areal biomass productivities of *P. tricornutum* cultures; (b) the specific energy dissipation rate and maximum acceptable culture velocity ($U_{L, max}$) to avoid shear stress related damage. The minimum velocity needed for well developed turbulence are also shown. The mean annual biomass productivity values were obtained by using the growth model (Ación Fernández et al., 1998), Eq. (1) and Eq. (3), with the following parameters: $n = 1.49$, $I_k = 114.67 \mu\text{E m}^{-2} \text{ s}^{-1}$, $K_a = 0.0369 \text{ m}^2 \text{ g}^{-1}$, and $\mu_{max} = 0.063 \text{ h}^{-1}$. The energy dissipation rate and culture velocity were obtained by using Eqs. (6)–(9).

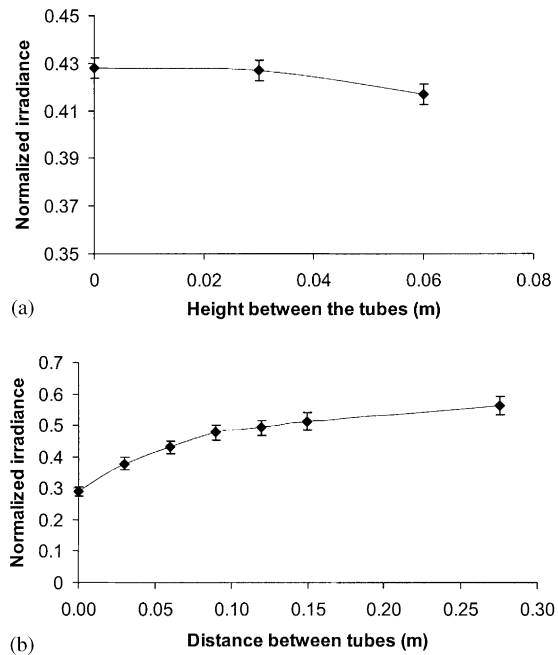


Fig. 4. Influence of the horizontal and vertical tube spacing on the irradiance received on the tubes surface relative to irradiance on the water pond. The data are the mean values from an analysis of variance of the measurements.

and minimum culture velocity available increased (Fig. 3b). Thus, to attain a compromise between the conflicting demands of volumetric and areal productivities, the energy dissipation per unit mass and the available culture velocity, a tube diameter value of 0.06 m was selected for construction. The estimated annual mean productivity for the selected tube diameter was $35 \text{ g m}^{-2} \text{ d}^{-1}$ or $1.5 \text{ g l}^{-1} \text{ d}^{-1}$, about 70% of the maximum value expected in a tube with a diameter of 0.03 m.

Regarding the optimal vertical and horizontal distances between adjacent tubes of the solar loop, the horizontal distance was found to be the main factor that influenced normalized irradiance (Fig. 4). Tubes spaced further apart horizontally (Fig. 4) received greater sunlight; however, once a spacing of about 0.1 m had been attained further increase did not significantly enhance the radiation received. Thus, a spacing of 0.09 m was selected for construction. The vertical distance between the two layers of tubes did not significantly affect the sunlight received; however, the irradiance was reduced slightly as the distance increased to 0.06 m (Fig. 4); thus, a lower value of 0.03 m was selected as satisfactory for construction of the solar loop. The noted geometry of the solar receiver enhanced light capture by 64% compared to if the tubes were installed parallel, in a single layer, directly on the floor with a white reflective coating on the floor, as previously used by Torzillo et al. (1993). The selected configuration reduced surface irradiance on tubes by only 17% compared to the single layer, parallel run

configuration with widely spaced tubes, as previously used by Molina Grima et al. (1994b).

As previously noted, excessive turbulence is potentially damaging to algal cells (Chisti, 1999b) and the culture velocity through the solar tubing is limited by shear stress considerations. Turbulence associated damage appears to occur when the dimensions of the terminal microeddies approach those of the algal cells (Torzillo et al., 1993; Contreras Gómez, García, Camacho, Molina Grima, & Merchuk, 1998). For *P. tricornutum*, Contreras Gómez et al. (1998) observed a decline in specific growth rate when the estimated dimensions of microeddies became $45 \mu\text{m}$ and lower. These dimensions are comparable to those of the *P. tricornutum* cells that are typically up to $35 \mu\text{m}$ long and $3 \mu\text{m}$ wide (Lewin, 1958). Thus, in the solar receiver tube, the flow velocity should be such that the microeddy dimensions remain greater than $45 \mu\text{m}$ (Molina Grima et al., 1999). If a lower safe limit on eddy length of $50 \mu\text{m}$ is accepted, the maximum culture velocity cannot exceed 1.0 m s^{-1} (Fig. 5), assuming a water-like behavior of the culture broth. The flow velocity to attain an eddy size of $50 \mu\text{m}$ is always greater than the threshold for laminar-turbulent transition. A velocity of 1.0 m s^{-1} corresponds to a specific power input of 0.17 W kg^{-1} , or 170 W m^{-3} . Although an upper velocity limit of 1.0 m s^{-1} was estimated, the design value was lower at 0.5 m s^{-1} because of limited mechanical strength of the plastic solar loop. Using this value of velocity, also in the turbulent regime, the maximum tube length was calculated such that the oxygen concentration at the end of the loop would not exceed 300% of air saturation value. The latter had been shown to be acceptable in earlier work (Ación Fernández et al., 1998; Camacho Rubio et al., 1999). Thus, a maximum oxygen generation rate of $0.003 \text{ mol O}_2 \text{ m}^{-3} \text{ s}^{-1}$, corresponding to a biomass productivity of $2.5 \text{ g l}^{-1} \text{ d}^{-1}$ (Ación Fernández et al., 1998), was used in Eq. (10) to obtain a maximum loop length of 80 m, for an assumed oxygen concentration of 100% of air saturation at the inlet of the loop.

The induced liquid circulation velocities for various aeration rates and heights of the airlift column were

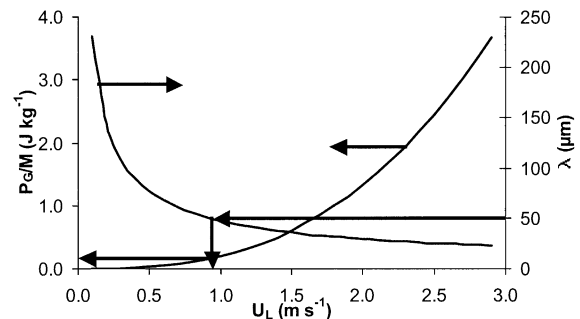


Fig. 5. Influence of liquid velocity on the length λ of the microeddies and power dissipation (consumption) for a 0.06 m diameter tube and a fluid with waterlike properties.

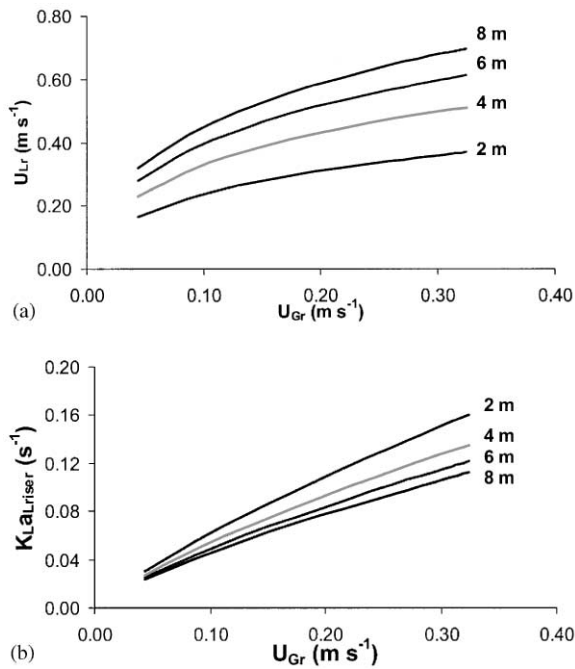


Fig. 6. Effects of superficial gas velocity (U_{Gr}) in the riser on: (a) the induced liquid velocity in the solar receiver tube; and (b) volumetric mass transfer coefficient (k_{LaL}) in the riser zone. The plots were simulated using Eqs. (16)–(20) for various heights of the airlift circulator.

simulated using Eqs. (16) and (17) to establish a satisfactory design height of the airlift column. Similarly, for the various selected gas injection rates in the airlift riser, the values of the mass transfer coefficient k_{LaL} were determined using Eqs. (17), (19), and (20). The results are shown in Fig. 6. As expected, for a given gas velocity in the riser and otherwise fixed conditions, the induced liquid circulation velocity increases as the height of the airlift column increases; however, as is obvious from Fig. 6a, the requisite liquid velocity of about 0.5 m s^{-1} cannot be attained with an airlift column that is less than 4 m tall for any reasonable gas flow rate. Thus, a 4 m airlift height was selected for construction. Also, for a 4 m tall airlift, the k_{LaL} value of 0.13 s^{-1} is easily attained in the airlift column (Fig. 6b). This value of k_{LaL} was estimated as being sufficient for reducing the dissolved oxygen concentration from 300% of air saturation to less than 150% of air saturation at the entrance of the solar receiver.

4.2. Hydrodynamic and mass transfer characterization

Once the photobioreactor had been built, its hydrodynamic and mass transfer behavior was characterized to validate the design approach used. Thus, the experimental measurements of the induced liquid velocity, the k_{LaL} and the dispersion coefficient values are shown in Fig. 7 for various values of the superficial aeration velocity in the riser. Separate k_{LaL} values are



Fig. 7. Effects of the superficial gas velocity U_{Gr} in the riser on: (a) the measured liquid velocity U_L in the loop; (b) the measured mass transfer coefficients, k_{LaL} ; and (c) the measured axial dispersion coefficient D_z . The k_{LaL} and D_z values are shown for the solar receiver tubing, the airlift device, and the airlift-loop combined (global) system.

shown for the airlift section and the tubular loop of the photobioreactor. Both the general behavior and the magnitude of the liquid velocity and the k_{LaL} data agree with the design predictions. The k_{LaL} values in the solar loop were of course much lower than ones in the airlift device (Fig. 7b) because the gas holdup and, consequently, the mass transfer interfacial area were minimal in the solar tube. Also, because the marginal gas holdup in the solar tube was little affected by the gas injection rate in the riser of the airlift device, the k_{LaL} in the loop was relatively insensitive to aeration rate. A relatively constant k_{LaL} in the loop also attests to a good gas-liquid separation performance of the degasser zone of the airlift device. As previously noted, the k_{LaL} in the airlift zone essentially controls the oxygen removal capability of the airlift column. The k_{LaL} in the solar loop influences the absorption of carbon dioxide injected in the loop.

The mixing performance of the photobioreactor was characterized in terms of the axial dispersion coefficients for the solar loop, the airlift zone, and an overall value for the airlift-loop combination. These various measured dispersion coefficients (D_z) are shown in Fig. 7c, as functions of the superficial gas velocity in the riser. Based on the dispersion coefficient values, the airlift device is clearly far better mixed than the solar tube. The mixing in the airlift zone improved as the gas flow rate increased. The solar tube, with low values of dispersion coefficients, was in plug flow and the dispersion coefficient was virtually constant irrespective of the liquid flow rate in the tube, or the aeration rate in the airlift riser zone.

Because of poor axial mixing in the solar loop, axial gradients in concentration of nutrients can develop. However, for most nutrients this was not an issue as the culture was continuously fed with fresh medium in the airlift device. The only nutrient that could become limiting in the solar loop was carbon dioxide that was injected near the entrance of the solar loop. Because the $k_L a_L$ value in the loop was low, pure carbon dioxide was indicated for injection to improve the gas-liquid mass transfer driving force and prevent carbon limitations (Camacho Rubio et al., 1999). However, injecting pure carbon dioxide can affect local pH values and culture productivity (Olaizola, Duerr, & Freeman, 1991; Mazuca Sobczuk et al., 2000). This effect may be reduced by diluting the injected gas with air or nitrogen. With careful attention to design, it is usually possible to ensure a sufficient mass transfer capability in the airlift device so that photosynthetically generated oxygen does not accumulate to excessively high concentrations. This capability was achieved as demonstrated during culture, discussed next.

4.3. Outdoor culture

In order to check the performance of the bioreactor the microalga *P. tricornutum* was cultured outdoors during Spring (Table 1). A biomass productivity of $1.2 \text{ g l}^{-1} \text{ d}^{-1}$ was obtained at a dilution rate of 0.050 h^{-1} when the mean solar irradiance on the pool (I_w) was about $1200 \mu\text{E m}^{-2} \text{ s}^{-1}$. (Note: the mean daily irradiance was calculated by time-averaging the instantaneous irradiance over a 24 h period.) The experimentally obtained biomass productivity of $1.2 \text{ g l}^{-1} \text{ d}^{-1}$ was about 10%

greater than the value estimated using the design methodology. A similar level of agreement was seen between the predicted and measured areal productivities of biomass, thus validating the predictive capability of the design equations.

To assess the influence of the solar loop liquid velocity on the culture performance, three different liquid velocities were tested: 0.50 , 0.35 , and 0.17 m s^{-1} , at a constant dilution rate of 0.050 h^{-1} . At the highest liquid velocity, the biomass concentration attained was 2.38 g l^{-1} . A lower concentration of 2.29 g l^{-1} was obtained when the velocity was reduced to 0.35 m s^{-1} ; however, the biomass productivity at these two velocities did not differ significantly. The culture carried out at a velocity of 0.17 m s^{-1} failed to attain steady state; the culture perished when the velocity was reduced further. Turbulence is known to enhance biomass productivity relative to laminar flow conditions. For example, Carozzi and Torzillo (1996) noted a lower biomass productivity in laminar flow relative to that in turbulent conditions for *Spirulina* cultures in tubular photobioreactors. A 29% increase in *Spirulina* biomass productivity was observed when the flow pattern changed from laminar to turbulent in straight tubes. Further improvement in turbulent mixing produced no beneficial effect; a high liquid velocity of 0.97 m s^{-1} damaged the culture and reduced the biomass productivity. Similar beneficial effects of limited turbulence have been also observed for *Chlorella* growing in a tubular photobioreactor (Pirt et al., 1983).

Turbulence repeatedly moves cells from darker interior of a tube to the better illuminated peripheral zone, hence the cells are not starved of light for extended periods. Also, movement of cells from light to dark zones may actually enhance productivity so long as the duration of a dark period remains small. Dark intervals of the order of 1 s are said to improve of the solar energy conversion by biomass (Laws, Satoru, Hirater, & Pang, 1987; Terry, 1986), as such intervals allow the dark catalytic reactions of photosynthesis to run to completion, restoring the photosynthetic apparatus to its full efficiency for the next light period. With *P. tricornutum* too, the biomass productivity increased with enhanced turbulence. Thus, as shown in Table 1, the biomass productivity was a little better at a higher flow velocity of 0.50 m s^{-1} compared to when the velocity was

Table 1

Biomass concentrations and productivities for various dilution rates, liquid velocities, and mean daily solar irradiance levels (Spring season) during cultures in the designed reactor.

Date	$D, \text{ h}^{-1}$	$U_L, \text{ m/s}$	$I_w (\mu\text{E m}^{-2} \text{ s}^{-1})$	$C_b, \text{ g/l}$	$P_{bc}, \text{ g/l d}$	$P_{ba}, \text{ g/m}^2 \text{ d}$
30/3	0.050	0.50	1289	2.38	1.19	19.8
5/4	0.050	0.35	1126	2.29	1.15	19.1
8/4	0.050	0.17	1250	—	—	—

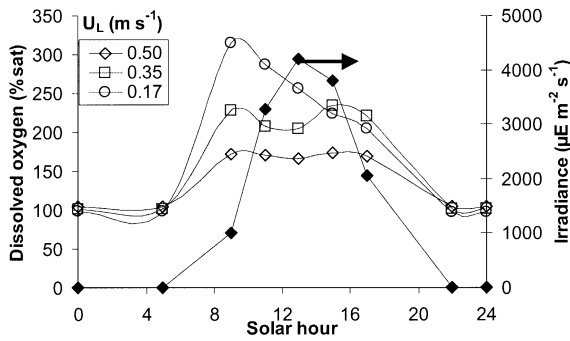


Fig. 8. Variation of solar irradiance and the dissolved oxygen concentration in the degasser zone with the solar hour. Data are shown for three different liquid velocities.

0.35 m s^{-1} . Potentially, this difference can be attributed to the small difference in irradiance between March and April (Table 1); however, the substantial change in productivity during April (Table 1) is clearly related with the velocity. As previously noted, the culture collapsed when the velocity was reduced to below 0.17 m s^{-1} , apparently because of photooxidation effects.

Liquid velocity also determines the maximum dissolved oxygen concentration developed in the tubular loop. This is because the residence time in the tube is governed by the velocity and the rate of generation of oxygen by photosynthesis is fixed under a given level of irradiance. The dissolved oxygen concentration in Fig. 8 varies because of a combined effect of the liquid velocity and the change in the irradiance level (Acien Fernández et al., 1998). During the early morning the dissolved oxygen concentration increases rapidly as irradiance increases to around $2500 \mu\text{E m}^{-2} \text{ s}^{-1}$. At midday, when the irradiance level exceeds $2500 \mu\text{E m}^{-2} \text{ s}^{-1}$, the dissolved oxygen declines because of a reduced rate of generation by photoinhibition. In the afternoon, as the solar irradiance decreases, the dissolved oxygen concentration also reduces. The maximum dissolved oxygen concentration attained is clearly influenced by the liquid velocity. Diurnal variation in concentration is minimal at the highest liquid velocity (Fig. 8).

5. Concluding remarks

A method is developed for design of airlift-driven photobioreactors with continuous run tubular solar loops. The design method effectively combines the relevant aspects of external irradiance-dependent cell growth, oxygen accumulation in the solar loop, oxygen removal in the airlift device, and hydrodynamics of the airlift system that determine the flow velocity through the solar receiver. A bioreactor configuration determined by the design methodology is proved during continuous outdoor culture of the microalga *P. tricorutum*. The

Table 2

Design and operation variables of the bioreactor for outdoor culture of microalgae

Description	Value
Tube diameter	0.06 m
Loop length	80 m
Culture volume	0.20 m^3
Land area occupied	12.0 m^2
Airlift column height	4 m
Vertical spacing between tube layers	0.03 m
Horizontal spacing between adjacent parallel tube rungs	0.09 m
Culture velocity through the solar tube	0.5 m s^{-1}
Superficial aeration velocity in the riser of the airlift	0.3 m s^{-1}

model predicted hydrodynamic behavior of the bioreactor agreed closely with the measured data. Similarly, the predicted culture productivity matched measurements. The designed bioreactor configuration and the suitable operations conditions are summarized in Table 2.

Notation

A_r	Cross sectional area of riser, m^2
A_D	Cross sectional area of degasser, m^2
A_d	Cross sectional area of downcomer, m^2
Bo	Bodenstein number in Eq. (23)
C	Tracer concentration, mol l^{-1}
C_b	Biomass concentration, g l^{-1}
C_f	Fanning friction factor
C_S	Concentration of suspended solids, g l^{-1}
C_0	Characteristic parameter in Eq. (17)
D	Dilution rate, h^{-1}
d	Horizontal spacing between tubes, m
d_B	Mean bubble diameter, m
D_L	Diffusivity of the transferring gas in liquid, $\text{m}^2 \text{ s}^{-1}$
D_z	Axial dispersion coefficient, $\text{m}^2 \text{ s}^{-1}$
F_{N_2}	Molar flow rate of the injected nitrogen, mol s^{-1}
g	Gravitational acceleration, m s^{-2}
h	Vertical spacing between tubes, m
h_D	Fluid height in the degasser, m
Δh_m	Manometer reading, m
h_r	Height of riser, m
h_t	Vertical distance between manometer taps, m
I_{av}	Average irradiance inside the reactor, $\mu\text{E m}^{-2} \text{ s}^{-1}$
I_k	Constant in Eq. (2), $\mu\text{E m}^{-2} \text{ s}^{-1}$
I_{mean}	Irradiance averaged over 24 h, $\mu\text{E m}^{-2} \text{ s}^{-1}$
$I_{normalized}$	Normalized irradiance
I_o	Irradiance on photobioreactor surface, $\mu\text{E m}^{-2} \text{ s}^{-1}$

I_w	Irradiance in the water pool, $\mu\text{E m}^{-2} \text{s}^{-1}$
J_r	Sum of superficial velocities of gas and liquid phases, m s^{-1}
$k_L a_L$	Volumetric gas–liquid mass transfer coefficient, s^{-1}
k_L	Gas–liquid mass transfer coefficient, m s^{-1}
K_a	Extinction coefficient for biomass, $\text{m}^2 \text{g}^{-1}$
K_B	Frictional loss coefficient for the bottom zone of the airlift
K_T	Frictional loss coefficient for the top of the airlift
L	Straight tube length in loop, m
L_D	Length of the degasser section, m
L_{eq}	Equivalent length of solar loop, m
L_{section}	Length of flow path in any zone, m
L_t	Distance between the tracer injection and detection points, m
M	Mass of liquid in reactor, kg
n	Exponent in Eq. (2)
n_T	Design specified factor in Eq. (5)
$[\text{O}_2^*]$	Saturation concentration of oxygen in liquid in equilibrium with gas phase, mol l^{-1}
$[\text{O}_2]_{\text{in}}$	Dissolved oxygen concentration at entrance of solar tube, mol l^{-1}
$[\text{O}_2]_{\text{out}}$	Dissolved oxygen concentration at the outlet of the solar tube, mol l^{-1}
P_{ba}	Areal productivity of biomass, $\text{g m}^{-2} \text{d}^{-1}$
P_{bv}	Volumetric productivity of biomass, g l^{-1}
P_G	Power input due to gassing, J s^{-1}
Q_G	Volumetric flow rate of gas in the riser zone, $\text{m}^3 \text{s}^{-1}$
Q_L	Volumetric flow rate of liquid, $\text{m}^3 \text{s}^{-1}$
Re	Reynolds number
Ro_2	Volumetric rate of oxygen generation, $\text{mol O}_2 \text{ m}^{-3} \text{ s}^{-1}$
t	Time, s
t_{mr}	Time interval between tracer injection and detection, s
U_b	Terminal rise velocity of single bubble, m s^{-1}
U_{Gr}	Gas velocity in the riser zone, m s^{-1}
U_L	Superficial liquid velocity in the tube, m s^{-1}
U_{LD}	Superficial liquid velocity in the degasser, m s^{-1}
V	Volume of culture, m^3
V_L	Volume of liquid in a given zone, m^3
Y_{O_2}	Oxygen-to-nitrogen molar ratio, $\text{mol O}_2 \text{ mol N}_2^{-1}$

Greek symbols

β	Ratio of superficial gas velocity to the total (gas and liquid) superficial velocity
ε_l	Gas holdup in the loop
ε_r	Gas holdup in the riser
ε_d	Gas holdup in the downcomer
λ	Length of microeddies, m

μ	Specific growth rate, h^{-1}
μ_L	Viscosity of the culture broth, $\text{kg m}^{-1} \text{s}^{-1}$
μ_{max}	Maximum specific growth rate, h^{-1}
ξ	Energy dissipation per unit mass, $\text{J s}^{-1} \text{kg}^{-1}$
ρ	Density of the fluid, kg m^{-3}
σ	Interfacial tension, J m^{-2}
ϕ	Solar tube diameter, m
ϕ_{eq}	Length of light path in Eq. (3) defined by Eq. (4), m
θ	Solar zenith angle in Eq. (4), deg

References

- Ación Fernández, F. G., García Camacho, F., Sánchez Pérez, J. A., Fernández Sevilla, J. M., & Molina Grima, E. (1997). A model for light distribution and average solar irradiance inside outdoor tubular photobioreactors for the microalgal mass culture. *Biotechnology and Bioengineering*, 55, 701–714.
- Ación Fernández, F. G., García Camacho, F., Sánchez Pérez, J. A., Fernández Sevilla, J. M., & Molina Grima, E. (1998). Modelling of biomass productivity in tubular photobioreactors for microalgal cultures: Effects of dilution rate, tube diameter and solar irradiance. *Biotechnology and Bioengineering*, 58, 605–616.
- Aiba, S. (1982). Growth kinetics of photosynthetic microorganisms. *Advances in Biochemical Engineering*, 23, 85–156.
- Alfano, O. M., Romero, R. L., & Cassano, A. E. (1986). Radiation field modelling in photoreactors—I. Homogeneous media. *Chemical Engineering Science*, 41, 421–444.
- Burlew, J. S. (1953). *Algal culture from laboratory to pilot plant*, vol. 600. Washington DC: Carnegie Institute.
- Camacho Rubio, F., Ación Fernández, F. G., Sánchez Pérez, J. A., García Camacho, F., & Molina Grima, E. (1999). Prediction of dissolved oxygen and carbon dioxide concentration profiles in tubular photobioreactors for microalgal culture. *Biotechnology and Bioengineering*, 62, 71–86.
- Carlozzi, P., & Torzillo, G. (1996). Productivity of Spirulina in a strongly curved outdoor tubular photobioreactor. *Applied Microbiology and Biotechnology*, 45, 18–23.
- Chisti, M. Y. (1989). *Airlift bioreactors*. London: Elsevier.
- Chisti, Y. (1999a). Mass transfer. In M. C. Flickinger, & S. W. Drew (Eds.), *Encyclopedia of bioprocess technology: Fermentation, biocatalysis and bioseparation*, vol. 3 (pp. 1607–1640). New York: Wiley.
- Chisti, Y. (1999b). Shear sensitivity. In M. C. Flickinger, & S. W. Drew (Eds.), *Encyclopedia of bioprocess technology: Fermentation, biocatalysis, and bioseparation*, vol. 5 (pp. 2379–2406). New York: Wiley.
- Chisti, M. Y., & Moo-Young, M. (1987). Airlift reactors: Characteristics, applications and design considerations. *Chemical Engineering Communications*, 60, 195–242.
- Chisti, Y., & Moo-Young, M. (1993). Improve the performance of airlift reactors. *Chemical Engineering Progress*, 89(6), 38–45.
- Contreras Gómez, A., García Camacho, F., Molina Grima, E., & Merchuk, J. C. (1998). Interaction between CO_2 –mass transfer, light availability, and hydrodynamic stress in the growth of *Phaeodactylum tricoratum* in a concentric tube airlift photobioreactor. *Biotechnology and Bioengineering*, 60, 317–325.
- Erickson, L. E., & Lee, H. Y. (1986). In W. Barclay, & R. P. McIntosh (Eds.), *Algal biomass technologies: An interdisciplinary perspective* (p. 197).
- Gudin, C., & Chaumont, D. (1983). Solar biotechnology study and development of tubular solar receptors for controlled production of photosynthetic cellular biomass. In W. Palz, & D. Pirrwitz (Eds.), *Proceedings of the Workshop and E. C. Contractor's meeting in Capri* (pp. 184–193). Dordrecht: D. Reidel Publishing Company.

- Incropera, F. P., & Thomas, J. F. (1978). A model for solar radiation conversion to algae in shallow pond. *Solar Energy*, 20, 157–165.
- Kawase, Y., & Moo-Young, M. (1990). Mathematical models for design of bioreactors: Applications of Kolmogoroff's theory of isotropic turbulence. *Chemical Engineering Journal*, 43, B19–B41.
- Lassen, C., & Jorgensen, B. (1994). A fiber optic irradiance microsensor (cosine collector): Application for in situ measurements of absorption coefficients in sediments and microbial mats. *FEMS Microbiology Ecology*, 15, 321–336.
- Laws, E. A., Satoru, T., Hirata, J., & Pang, L. (1987). Optimization of microalgae production in a shallow outdoor flume. *Biotechnology and Bioengineering*, 32, 140–147.
- Lewin, J. C. (1958). The taxonomic position of *Phaeodactylum tricornutum*. *Journal of General Microbiology*, 18, 427–432.
- Mann, J. E., & Myers, J. (1968). On pigments, growth and photosynthesis of *Phaeodactylum tricornutum*. *Journal of Phycology*, 4, 349–355.
- Mazzuca Sobczuk, T., García Camacho, F., Camacho Rubio, F., Ación Fernández, F. G., & Molina Grima, E. (2000). Carbon dioxide uptake efficiency by outdoor microalgal cultures in tubular airlift photobioreactors. *Biotechnology and Bioengineering*, 67, 465–475.
- Molina Grima, E. (1999). Microalgae, mass culture methods. In M. C. Flickinger, & S. W. Drew (Eds.), *Encyclopedia of bioprocess technology: Fermentation, biocatalysis and bioseparation*, vol. 3 (pp. 1753–1769). New York: Wiley.
- Molina Grima, E., Ación Fernández, F. G., García Camacho, F., & Chisti, Y. (1999). Photobioreactors: Light regime, mass transfer, and scale up. *Journal of Biotechnology*, 70, 231–248.
- Molina Grima, E., García Camacho, F., Sánchez Pérez, J. A., Fernández Sevilla, J. M., Ación Fernández, F. G., & Contreras Gómez, A. (1994a). A mathematical model of microalgal growth in light limited chemostat culture. *Journal of Chemical Technology and Biotechnology*, 61, 167–173.
- Molina Grima, E., García Camacho, F., Sanchez Perez, J. A., Urda Cardona, J., Ación Fernández, F. G., & Fernández Sevilla, J. M. (1994b). Outdoor chemostat culture of *Phaeodactylum tricornutum* UTEX 640 in a tubular photobioreactor for the production of eicosapentaenoic acid. *Biotechnology and Applied Biochemistry*, 20, 279–290.
- Olaizola, M., Duerr, E. O., & Freeman, D. W. (1991). Effect of CO₂ enhancement in an outdoor algal production system using *Tetraselmis*. *Journal of Applied Phycology*, 3, 363–366.
- Pirt, S. L., Lee, Y. K., Walach, M. R., Pirt, M. W., Balyuzi, H. H., & Bazin, M. J. (1983). A tubular bioreactor for photosynthetic production of biomass from carbon dioxide: Design and performance. *Journal of Chemical Technology and Biotechnology*, 33B, 35–58.
- Rorrer, G. L., & Mullikin, R. K. (1999). Modeling and simulation of a tubular recycle photobioreactor for macroalgal cell suspension cultures. *Chemical Engineering Science*, 54, 3153–3162.
- Terry, K. L. (1986). Photosynthesis in modulated light: Quantitative dependence of photosynthetic enhancement on flashing rate. *Biotechnology and Bioengineering*, 28, 988–995.
- Tredici, M. R. (1999). Bioreactors, photo. In M. C. Flickinger, & S. W. Drew (Eds.), *Encyclopedia of bioprocess technology: Fermentation, biocatalysis and bioseparation*, vol. 1 (pp. 395–419). New York: Wiley.
- Torzillo, G., Carozzi, P., Pushparaj, B., Montaini, E., & Materassi, R. (1993). A two plane tubular photobioreactor for outdoor culture of *Spirulina*. *Biotechnology and Bioengineering*, 42, 891–898.
- Torzillo, G., Pushparaj, B., Bocci, F., Balloni, W., Materassi, R., & Florenzano, G. (1986). Production of *Spirulina* biomass in closed photobioreactors. *Biomass*, 11, 61–64.
- Verlaan, P., Van Eijs, A. M. M., Tramper, J., & van't Riet, K. (1989). Estimation of axial dispersion in individual sections of an airlift-loop reactor. *Chemical Engineering Science*, 44, 1139–1146.
- Weissman, J. C., Goebel, R. P., & Benemann, J. R. (1988). Photobioreactor design: Mixing, carbon utilization, and oxygen accumulation. *Biotechnology and Bioengineering*, 31, 336–344.
- Zuber, N., & Findlay, J. A. (1965). Average volumetric concentration in two phase flow systems. *Journal of Heat Transfer ASME*, 453–457.